

Formation of high-speed electron jets as the evidence for magnetic reconnection in laser-produced plasma


Kai Huang, Can Huang, Quanli Dong, Quanming Lu, San Lu, Zhengming Sheng, Shui Wang, and Jie Zhang

Citation: *Physics of Plasmas* **24**, 041406 (2017); doi: 10.1063/1.4978883

View online: <http://dx.doi.org/10.1063/1.4978883>

View Table of Contents: <http://aip.scitation.org/toc/php/24/4>

Published by the *American Institute of Physics*



Small Conferences. BIG Ideas.

Applied Physics
Reviews

SAVE THE DATE!
3D Bioprinting: Physical and Chemical Processes
May 2–3, 2017 • Winston Salem, NC, USA

The background of the banner features a blue-toned image of a human hand holding a glowing, branching structure that resembles a biological or chemical process, possibly related to bioprinting or plasma physics.

Formation of high-speed electron jets as the evidence for magnetic reconnection in laser-produced plasma

Kai Huang,^{1,2} Can Huang,^{1,2,a)} Quanli Dong,^{3,4,a)} Quanming Lu,^{1,2} San Lu,⁵
 Zhengming Sheng,^{6,7,4} Shui Wang,^{1,2} and Jie Zhang^{6,4}

¹CAS Key Lab of Geospace Environment, Department of Geophysics and Planetary Science, University of Science and Technology of China, Hefei 230026, China

²Collaborative Innovation Center of Astronautical Science and Technology, Hefei 230026, China

³School of Physics and Optoelectronic Engineering, Ludong University, Yantai 264025, China

⁴Innovative Collaboration Center of IFSA, Shanghai Jiao Tong University, Shanghai 200240, China

⁵Department of Earth, Planetary, and Space Sciences, and Institute of Geophysics and Planetary Physics, University of California, Los Angeles, California 90095, USA

⁶MoE Key Laboratory for Laser Plasmas and Department of Physics, Shanghai Jiao Tong University, Shanghai 200240, China

⁷SUPA, Department of Physics, University of Strathclyde, Glasgow G4 0NG, United Kingdom

(Received 13 October 2016; accepted 27 December 2016; published online 27 March 2017)

Experiments about the flow-driven magnetic reconnection in high-energy-density laser-produced plasmas have recently been conducted on different platforms of giant laser facilities. In this paper, we perform two-dimensional (2D) particle-in-cell simulations to study the interactions of two colliding laser-produced plasma bubbles with a self-generated toroidal magnetic field. Two cases are investigated: in one case, the two plasma bubbles have an anti-parallel magnetic field (AP-case) in the colliding region, and in the other case, the two interacting parts of the magnetic field are configured parallel to each other (P-case). In both cases, the quadrupole structure of the out-of-plane magnetic field is observed, as well as the Hall electric field and the electron energization in the colliding region. However, only in the AP-case, three well-collimated in-plane electron jets are observed. Two electron jets along the magnetic field at the edge of the plasma bubbles are formed because the electrons are trapped and accelerated by the out-of-plane electric field located between the two colliding bubbles and then move outward along the magnetic field. The high-speed electron jet in the middle of the outflow region is formed as the electrons are reflected and accelerated in the pileup region of the magnetic field, which is moving outward quickly. We demonstrate that besides the annihilation of the magnetic field in the colliding region between the two laser-produced plasma bubbles approaching each other, the three well-collimated electron jets can also be considered as the evidence for the magnetic reconnection. *Published by AIP Publishing.*

[<http://dx.doi.org/10.1063/1.4978883>]

I. INTRODUCTION

Magnetic reconnection is a fundamental physical process in plasmas, during which the topology of magnetic field lines is rearranged and magnetic energy is converted to plasma kinetic energy.^{1–4} This process is generally invoked to explain the explosive phenomena in different plasma environments, such as solar flares,^{5,6} substorms in Earth's magnetosphere,^{7–9} and sawtooth crashes in tokamaks.^{10,11} Much of the electron dynamics in the magnetic reconnection process has been learned from particle simulations^{12–19} and *in situ* satellite observations of Earth's magnetosphere.^{20–27} Super-Alfvénic electron jets are found to be one of the important characteristics in magnetic reconnection.^{28–33} In most studies, two high-speed jets are formed in the outflow region of magnetic reconnection after they are accelerated in the vicinity of the X line by the reconnection electric field and then run away along the magnetic field that helps form the separatrixes.³³

Recently, magnetic reconnection experiments in high-energy-density (HED) laser-produced plasmas have been conducted on different platforms of Vulcan,^{34–36} OMEGA,^{37,38} and Shenguang-II (SG-II) facilities,^{39,40} respectively. In such laser-driven magnetic reconnection, two plasma bubbles are produced side-by-side by two HED laser beams focused on a planar foil target. In the overlapping region of the two plasma bubbles, the azimuthal spontaneous magnetic fields produced in each bubble due to the well-known Biermann effects are then inherently configured as anti-parallel so that there occurs the reconnection of these two approaching magnetic field lines. The squeezing of the two plasma bubbles and the resultant compression of the magnetic fields due to the strong counter streaming plasma inflow there are expected to play significant roles in such laser-driven reconnection.^{41,42} Although both laser-driven magnetic reconnection experiments and particle-in-cell (PIC) simulations based on corresponding experimental parameters have demonstrated the formation of high-speed electron jets in the outflow region,^{35,38,40,43,44} there is still speculation

^{a)}Authors to whom correspondence should be addressed. Electronic addresses: canhuang@mail.ustc.edu.cn and qldong@aphy.iphy.ac.cn

whether the high-speed electron jets could be created merely by the plasma bubble collision without magnetic reconnection.

In this paper, we perform two-dimensional (2D) PIC simulations to revisit the interactions of two colliding laser-produced plasma bubbles with self-generated toroidal magnetic fields. Two geometries of the magnetic field lines in the colliding region are investigated with the two interacting sets of magnetic fields in each case configured as anti-parallel or parallel to their correspondents. The two geometries are referred hereafter as the AP-case and the P-case, respectively. Of course, no reconnection is expected in the latter case. By comparing the two cases, we find that high-speed electron jets can only be formed when the magnetic reconnection occurs between the two bubbles and demonstrate that high-speed electron jets can be considered to be the evidence of laser-driven magnetic reconnection.

The outline of the paper is organized as follows: In Sec. II, the simulation model is described, and Sec. III presents the simulation results. At last, the conclusions and discussion are given in Sec. IV.

II. SIMULATION MODEL

In our 2D PIC simulation model, the electromagnetic field is defined on the grids and updated by solving Maxwell's equations with a full explicit algorithm. Ions and electrons are relativistically advanced in the electromagnetic field. The processes of laser-plasma interactions and magnetic generation are not included in the simulations, and the initial conditions of the simulations are set corresponding to the plasma bubble expanding phase in the experiment.^{41,45}

Two circular plasma bubbles are defined in the (x, z) plane with a toroidal magnetic field around it. The simulation domain size is $[-L_x, L_x] \times [-L_z, L_z]$, and the centers of the two plasma bubbles locate at $(0, -L_0)$ and $(0, L_0)$, respectively, from which their radius vectors are defined as $\mathbf{r}^{(1)} = (x, z + L_0)$ and $\mathbf{r}^{(2)} = (x, z - L_0)$ accordingly. The initial density is defined as $n_b + n^{(1)} + n^{(2)}$, where n_b is the background density and $n^{(i)} (i = 1, 2)$ is the density of each bubble with the following distributions:

$$n^{(i)}(\mathbf{r}) = \begin{cases} (n_0 - n_b) \cos^2\left(\frac{\pi r^{(i)}}{2L_n}\right) & \text{if } r^{(i)} < L_n, \\ 0 & \text{otherwise.} \end{cases} \quad (1)$$

Here, L_n is the radius of the two bubbles, and $L_n < \min\{L_0, L_x\}$ and $L_0 + L_n < L_z$, so that the simulation domain can contain two whole bubbles. n_0 is the peak density of two plasma bubbles, and $n_b = 0.1n_0$ is chosen. The initial expanding velocity of the plasma bubbles is $\mathbf{V}^{(1)} + \mathbf{V}^{(2)}$, and $\mathbf{V}^{(i)} (i = 1, 2)$ is

$$\mathbf{V}^{(i)}(\mathbf{r}) = \begin{cases} V_0 \sin\left(\frac{\pi r^{(i)}}{L_n}\right) \hat{\mathbf{r}}^{(i)} & \text{if } r^{(i)} < L_n, \\ 0 & \text{otherwise.} \end{cases} \quad (2)$$

The magnetic field, which is the sum of two toroidal ribbons, $\mathbf{B}^{(1)} + \mathbf{B}^{(2)}$, bears the only initialization difference between the AP-case and the P-case.

In the AP-case, the magnetic field is defined as

$$\mathbf{B}^{(i)}(\mathbf{r}) = \begin{cases} B_0 \sin\left(\frac{\pi(L_n - r^{(i)})}{2L_B}\right) \hat{\mathbf{r}}^{(i)} \times \hat{\mathbf{y}} & \text{if } r^{(i)} \in [L_n - 2L_B, L_B], \\ 0 & \text{otherwise,} \end{cases} \quad (3)$$

where L_B is the half width of the initial magnetic ribbons.

In the P-case, the magnetic field is

$$\mathbf{B}^{(i)}(\mathbf{r}) = \begin{cases} B_0 \sin\left(\frac{\pi(L_n - r^{(1)})}{2L_B}\right) \hat{\mathbf{r}}^{(1)} \times \hat{\mathbf{y}} & \text{if } r^{(1)} \in [L_n - 2L_B, L_B], \\ -B_0 \sin\left(\frac{\pi(L_n - r^{(2)})}{2L_B}\right) \hat{\mathbf{r}}^{(2)} \times \hat{\mathbf{y}} & \text{if } r^{(2)} \in [L_n - 2L_B, L_B], \\ 0 & \text{otherwise.} \end{cases} \quad (4)$$

An initial out-of-plane current is added to satisfy Ampere's law. Moreover, to be consistent with the plasma flow, an initial electric field $\mathbf{E} = -\mathbf{V} \times \mathbf{B}$ is imposed.

The size of the plasma bubbles is $L_n = 12d_i$, and $L_0 = 12.5d_i$ in our simulations, where $d_i = c/\omega_{pi}$ is the ion inertial length based on n_0 , and $L_B = 2d_i$. The mass ratio is $m_i/m_e = 400$, and the light speed is $c/v_A = 75$, where v_A is the Alfvén speed based on n_0 and B_0 . The initial temperature of all ions and electrons is set to be uniform

$T_i = T_e = 0.1m_e c^2$, and their initial velocity distributions are Maxwellian with the bulk velocities in the radial direction and the drift velocities in the y direction to supply the out-of-plane current. The expanding speed of the plasma bubbles is usually supersonic, and here we set the plasma expanding velocity $V_0 = 4.6v_A$ and the ionic charge $Z = 10$. The electron plasma beta is $\beta_e = 2\mu_0 n_0 k_B T_e / B_0^2 \approx 2.9$. In the simulations, $L_x = 25.5d_i$ and $L_z = 35d_i$, and the number of grid points is $N_x \times N_z = 2040 \times 2800$ with a spatial resolution of

$\Delta x = \Delta z = 0.025d_i$. The time step is $\Delta t = 0.00005\Omega_i^{-1}$, where $\Omega_i = eB_0/m_i$ is the ion gyrofrequency. 640 particles per species in a grid for n_0 are employed in the simulations. The periodic boundary condition is applied in both x and z directions. Compared with the experiments, e.g., the SG-II reconnection ones,^{40,46} parameters utilized above correspond to the following experimental conditions: the peak ion density $n_{i0} \sim 5 \times 10^{19} \text{ cm}^{-3}$, the magnetic field $B_0 \sim 2 \text{ MG}$, and the Al foil target. Then, the ion inertial length $d_i \sim 16.8 \mu\text{m}$, $L_B \sim 33.6 \mu\text{m}$, the plasma bubble size $L_n \sim 201.6 \mu\text{m}$, the Alfvén speed $v_A \sim 1.2 \times 10^5 \text{ ms}^{-1}$, and the plasma expanding speed $V_0 \sim 5.5 \times 10^5 \text{ ms}^{-1}$.

III. SIMULATION RESULTS

We at first introduce the results of the AP-case with magnetic reconnection. Figure 1 shows the time evolution of the magnetic field B/B_0 and the out-of-plane electron current density J_{ey}/n_0ev_A . The in-plane magnetic field lines are also plotted for reference. The process can be roughly divided into two stages. In the first stage, the two magnetic ribbons squeeze each other due to the high expanding speed of the plasma bubbles. As demonstrated by Lu *et al.*,⁴² because the expanding speed of the plasma bubbles is much higher than the local Alfvén speed, the magnetic flux pileup is faster than the reconnection rate. The toroidal magnetic field associated with the plasma bubbles can be enhanced about 2–3 times the initial value, and simultaneously, a thin current sheet is formed. Subsequently, in the second stage, magnetic reconnection occurs at about $\Omega_i t = 1.1$ when the expansion

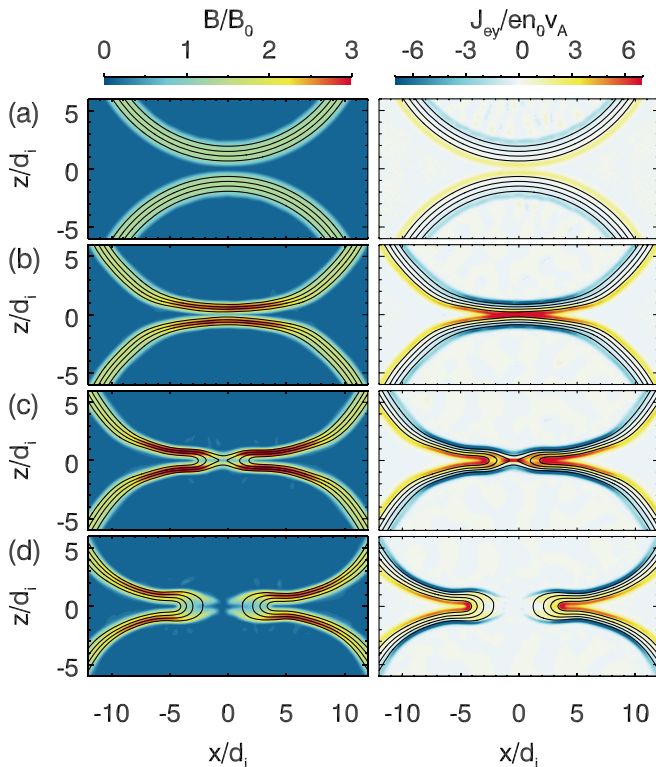


FIG. 1. Time evolution of the magnetic field B/B_0 and the out-of-plane electron current density J_{ey}/en_0v_A at $\Omega_i t =$ (a) 0.5, (b) 1.0, (c) 1.3, and (d) 1.6, respectively. The in-plane magnetic field lines are also plotted for reference.

of the plasma bubbles and then the magnetic flux pileup have been significantly slowed down.

Figure 2 plots the time evolution of the reconnected magnetic flux Φ_B/B_0d_i and the reconnection electric field E_y/v_AB_0 at the X-line. The peak value of the reconnection electric field can reach $5.0 v_AB_0$, which is much larger than with a Harris current sheet. This is attributed to the squeezing of the plasma bubbles as explained by Fox *et al.*⁴¹ As the toroidal magnetic field associated with the plasma bubbles piled up, the local Alfvén speed is greatly enhanced to be much larger than its initial values when reconnection occurs. In our simulations, if we normalized the reconnection electric field to the instantaneous values of the Alfvén speed and magnetic field in the upstream of the X line as shown by the dotted line in Fig. 2, its peak varies between 0.1 and 1, which is consistent with the prediction in the Harris current sheet. However, in the saturation stage of magnetic reconnection, all the magnetic flux in the upstream is reconnected and then expelled into the downstream, and the magnetic field in the upstream approaches zero. Therefore, in the saturation stage, it cannot give useful information if we normalize the reconnection electric field to the instantaneous values of the Alfvén speed and magnetic field in the upstream of the X line. Therefore, in the situation of flow-driven laser-plasma magnetic reconnection, it is preferred to normalize physical values with the background magnetic field and corresponding Alfvén speed rather than the instantaneous ones in the vicinity of the X-line so that a continuous and comprehensive description of the physical process can be achieved.

In order to distinguish the differences between the AP-case and the P-case, we compare the magnetic field B/B_0 , the out-of-plane magnetic field B_y/B_0 , the out-of-plane electron current density J_{ey}/n_0ev_A , the electric field in the z direction E_z/v_AB_0 , and the electron temperature $T_e/m_iv_A^2$ in the two cases. Figures 3 and 4 plot these values at two different times $\Omega_i t = 1.0$ and 1.3 . The in-plane magnetic field lines are also plotted in the figures for reference. In the P-case, there is only the squeezing of the two colliding plasma bubbles and magnetic ribbons, while in the AP-case, we can observe the topological change in magnetic field lines. In the AP-case, recorded physical variables at the times $\Omega_i t = 1.0$ and 1.3 represent the squeezing and reconnection stages, respectively. In both cases, because the curvature radii of the plasma bubbles are on the order of the ion gyro-radius, the electrons are frozen around the magnetic field lines except in

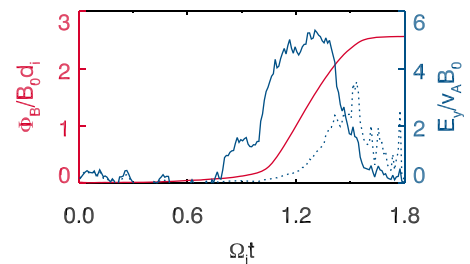


FIG. 2. Time evolution of the reconnected magnetic flux Φ_B/B_0d_i and the reconnection electric field E_y/v_AB_0 at the X-line $((x, z) = (0, 0))$. The reconnection electric field normalized to the Alfvén speed and magnetic field in the upstream of the X line is also shown as the dotted line for comparisons.

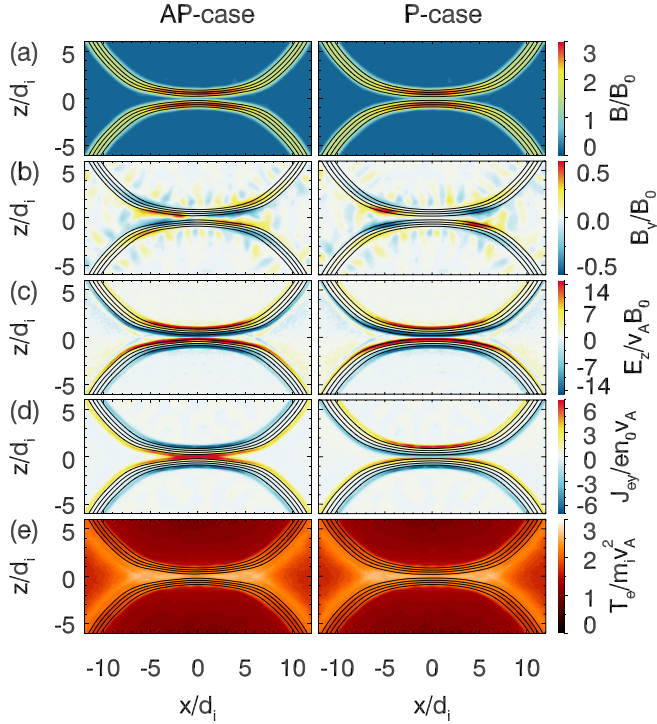


FIG. 3. Comparison between the AP-case and the P-case at the expanding or squeezing stage at $\Omega_i t = 1.0$: (a) the magnetic field B/B_0 , (b) the out-of-plane magnetic field B_y/B_0 , (c) the electric field in the z direction $E_z/v_A B_0$, (d) the out-of-plane electron current density $J_{ey}/en_0 v_A$, and (e) the electron temperature $T_e/m_i v_A^2$.

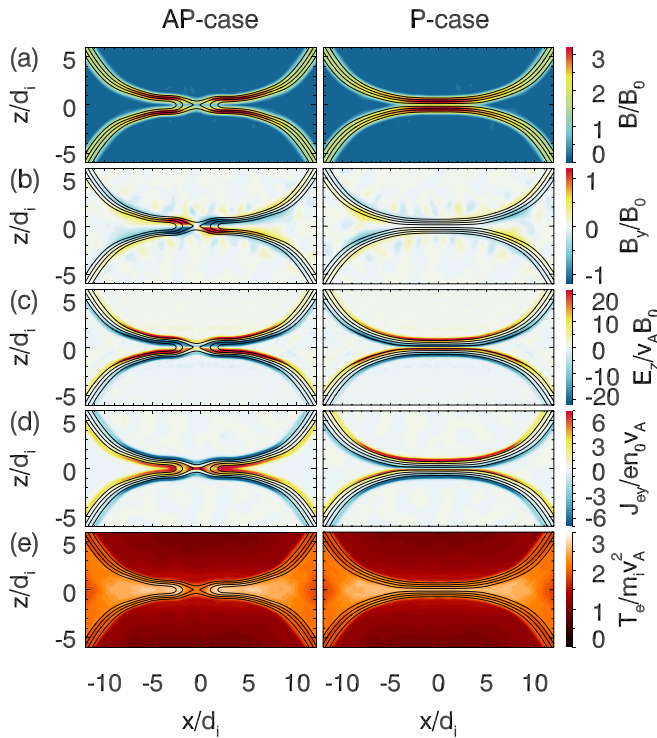


FIG. 4. Comparison between the AP-case and the P-case at the reconnection stage at $\Omega_i t = 1.3$: (a) the magnetic field B/B_0 , (b) the out-of-plane magnetic field B_y/B_0 , (c) the electric field in the z direction $E_z/v_A B_0$, (d) the out-of-plane electron current density $J_{ey}/en_0 v_A$, and (e) the electron temperature $T_e/m_i v_A^2$.

the electron diffusion region (EDR) during the reconnection stage for the AP case, while the ions are not magnetized. This feature results in the generation of the local net charge and then the Hall electric field E_z at the edge of the plasma bubbles, as well as the quadrupole structures of the out-of-plane magnetic field. It is noted that the generation of the quadrupole out-of-plane magnetic field is not the sufficient condition for the occurrence of reconnection here, as also mentioned in recent works.⁴⁸ Also, in both cases, part of electrons is energized at the ribbon of the plasma bubbles through the betatron mechanism due to the enhancement of the magnetic field, while part of electrons is trapped and gets energized through the Fermi mechanism. As demonstrated in Ref. 46, the betatron mechanism together with the Fermi mechanism dominates the process of electron energization before the reconnection occurs. Therefore, the enhancement of the electron temperature is also similar in the AP-case and the P-case. These results have also been discussed in Ref. 47. However, only in the AP-case, we can observe the enhancement of the out-of-plane electron current density in the vicinity of the X line.

For the reconnection studies, it is critical to analyze the diffusion region where charged particles are decoupled from the field lines. In simulations, the measurement of the curl of the non-ideal electric field $\nabla \times (\mathbf{E} + \mathbf{V}_{i,e} \times \mathbf{B})$ can be treated as a criterion of the diffusion region. Figures 5(a) and 5(b) show the curl of the non-ideal electric field in the ion's and electron's frames, respectively. The scale of the ion diffusion region, which covers the whole reconnection site, is about $10 d_i$ in the x direction and $3 d_i$ in the z direction. Its position corresponds to the quadrupole out-of-plane magnetic field in Fig. 3. Meanwhile, the electron diffusion region (EDR) is embedded in the center of the ion diffusion region and has a smaller scale of about $4 d_i$ in the x direction and $1 d_i$ in the z direction. This picture is similar to that of the reconnection in a Harris sheet. The same quantities are also shown for the P-case, but there are no obvious signatures for ion or electron diffusion regions. The electron agyrotropy, an alternative measurement of the EDR as proposed by Scudder and Daughton,⁴⁹ is plotted in Figure 5(c). The width of EDR in

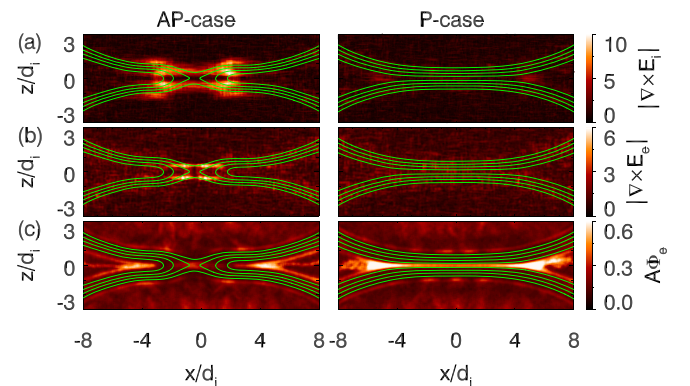


FIG. 5. Contours of (a) the absolute value of the curl of non-ideal electric field $\mathbf{E}_i = \mathbf{E} + \mathbf{V}_i \times \mathbf{B}$, (b) the absolute value of the curl of non-ideal electric field $\mathbf{E}_e = \mathbf{E} + \mathbf{V}_e \times \mathbf{B}$, and (c) the electron agyrotropy $A\Phi_e$, in the AP-case and the P-case, respectively.

this measurement is narrower than the curl of the non-ideal electric field. It is noted that the agyrotropy is large along the edge of magnetic ribbons, especially in front of the piled-up magnetic field lines in the outflow region, so does it in the P-case. The increase in electron agyrotropy in these regions is attributed to the large gradient of the magnetic field and small radius of the curvature of the magnetic field lines. This is the one feature that makes the magnetic reconnection differ in the laser produced plasma from that in a Harris sheet. In the AP-case, however, a third electron agyrotropy peak area is observed in the middle of the outflow region, which is absent in the P-case. Such a feature also has its correspondent in the electron velocity distribution as shown below.

The parallel electric field in the vicinity of the X-line in the AP-case is also diagnosed. Figure 6(a) shows that in the ion diffusion region, there is a parallel electric field, which around the EDR also has a large scale quadrupole structure, i.e., the direction of this large scale parallel electric field is reversed along the horizontal (x) and vertical (z) directions near the X-line. Contributions of the electron pressure term $(-\nabla \cdot \mathbb{P}_e/ne)_{\parallel}$ and the electron inertial term $(-m_e d\mathbf{V}_e/dt)_{\parallel}$ in the generalized Ohm's law are also plotted (where \mathbb{P}_e is the electron pressure tensor) in Figs. 6(b) and 6(c), respectively. The comparisons between the three graphed variables along the dashed line in Figs. 6(a)–6(c) are shown in Figs. 6(d)–6(f), indicating that the contribution from the divergence of electron pressure tensor dominates the large scale parallel electric field. This kind of pressure distribution and the parallel electric field are caused by the non-adiabatic motion of electrons when the upstream electron β becomes significantly low, as described by Egedal *et al.*⁵⁰ and Huang *et al.*⁵¹

Figure 7 shows the evolution of the in-plane electron jets V_{ein}/v_A (Fig. 7(a)) and the out-of-plane electric field $E_y/v_A B_0$ (Fig. 7(b)) in the AP-case. With the proceeding of magnetic reconnection, the electrons are accelerated by the reconnection electric field in the vicinity of the X line. When

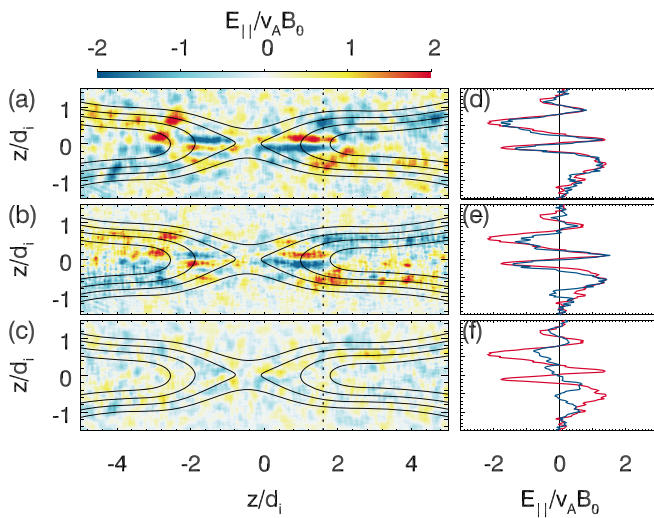


FIG. 6. Contours of (a) the parallel electric field $E_{\parallel}/v_A B_0$, (b) the electron pressure term, and (c) the electron inertial term. The red line in (d)–(f) shows the $E_{\parallel}/v_A B_0$ along the dotted line at $x = 1.6d_i$ in (a)–(c). The blue lines in (e) and (f) show the electron pressure term and the electron inertial term along the same line, respectively, while the blue line in (d) shows the sum of the pressure term and the inertial term in (e) and (f).

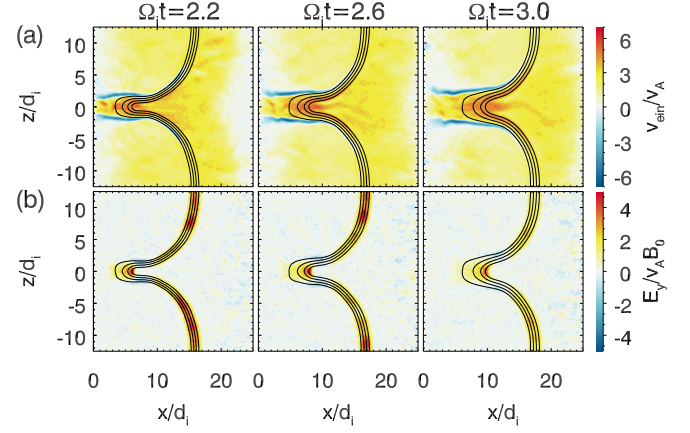


FIG. 7. Contours of (a) the in-plane electron flow velocity V_{ein}/v_A and (b) the out-of-plane electric field $E_y/v_A B_0$ at $\Omega_2 t = 2.2, 2.6,$ and 3.0 in the AP-case. V_{ein} is defined as $V_{ein} = \text{sgn}(V_{ex}) \cdot \sqrt{V_{ex}^2 + V_{ez}^2}$, in which V_{ex} and V_{ez} are the electron flow velocities in the x and z directions, and $\text{sgn}(x)$ is the sign function. The in-plane magnetic field lines are plotted for reference.

they are directed away from the X line, two electron jets along the magnetic field at the edge of the plasma bubbles are formed. At the later stage of the reconnection, a third electron jet directed away from the X line is formed in the middle of the outflow region between two plasma bubbles. The electron jet in the middle is formed as the electrons are reflected by the piled-up magnetic field, which moves away from the X line quickly. The three-tined fork structure of the electron in-plane velocity distribution is the same as that of the electron agyrotropy and consists of the important feature of the electron diffusion regions. Such a feature is also observed in other PIC simulations,³⁰ in satellite measurements of magnetic reconnections in Earth's magnetosphere,³¹ and in laser-plasma experiments.⁴⁰ But obviously, more experimental results are necessary for this EDR feature study. As comparison, Fig. 8 shows the evolution of the in-plane electron jets V_{ein}/v_A and the out-of-plane electric field $E_y/v_A B_0$ in the P-case. In the colliding region between the two plasma bubbles, there is neither obvious electric field in the out-of-plane direction nor obvious electron jets.

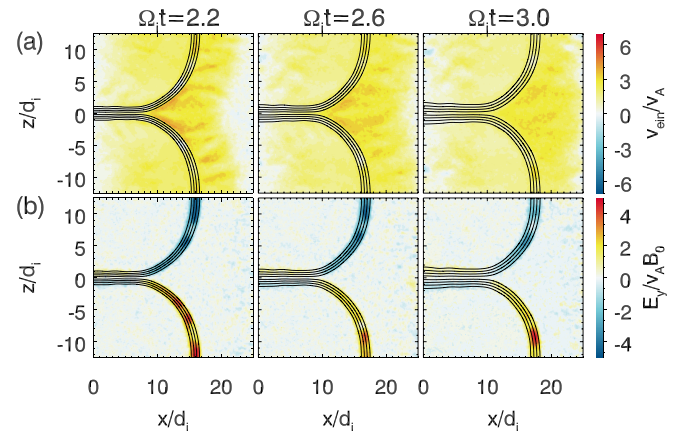


FIG. 8. Contours of (a) the in-plane electron flow velocity V_{ein}/v_A and (b) the out-of-plane electric field $E_y/v_A B_0$ at $\Omega_2 t = 2.2, 2.6,$ and 3.0 in the P-case. V_{ein} is defined as in Figure 7. The in-plane magnetic field lines are plotted for reference.

IV. CONCLUSIONS AND DISCUSSION

In this paper, we perform 2D PIC simulations to study the interactions between laser-produced plasma bubbles. By comparing the results from the AP-case and the P-case, we find that in both cases, there exist the quadruple structure of the out-of-plane magnetic field, the Hall electric field due to the separation of ion motions from electrons, and the enhancement of the electron temperature. However, the characteristics of the in-plane electron jets in the two cases are different. In the AP-case, besides the two electron jets, which are directed away from the colliding region along the magnetic field at the edges of the plasma bubbles, there is still a third electron jet in the middle of the outflow region. The two electron jets at the edges of the plasma bubbles are formed as the electrons are trapped and accelerated by the out-of-plane electric field between the colliding bubbles and then leave outward along the magnetic field. The electron jet in the middle is formed by the electrons that are reflected and accelerated by the magnetic field in the pileup region, which is moving outward quickly. In the P-case, obvious electron jets are not observed.

The magnetic reconnection occurring in two laser-produced plasma bubbles needs further investigations. The annihilation of the magnetic field in this kind of experiments was observed by Li *et al.*³⁷ In the following experiments, both Dong *et al.*⁴⁰ and Rosenberg *et al.*⁵² observed three well-collimated high-speed plasma/electron jets, which bear similar features but obtained through different diagnostics and using the Shenguang-II (SG-II) and the Omega laser facilities, respectively. Our simulations reproduce both the magnetic annihilation and the three plasma/electron jets, which leads to a conclusion that the well collimated electron jets can be regarded as the evidence of magnetic reconnection.

ACKNOWLEDGMENTS

This work was supported by 973 Program (2013CBA01503), the National Science Foundation of China, Grant Nos. 41331067, 11274152, 41527804, 41121003, and 11220101002, and the Key Research Program of Frontier Sciences, CAS(QYZDJ-SSW-DQC010).

- ¹D. Biskamp, *Magnetic Reconnection in Plasmas* (Cambridge University Press, Cambridge, 2000).
- ²J. Birn and E. R. Priest, *Reconnection of Magnetic Fields: Magnetohydrodynamics and Collisionless Theory and Observations* (Cambridge University Press, Cambridge, 2007).
- ³M. Yamada, R. Kulsrud, and H. T. Ji, *Rev. Mod. Phys.* **82**, 603 (2010).
- ⁴S. Lu, Q. M. Lu, C. Huang, and S. Wang, *Phys. Plasmas* **20**, 061203 (2013).
- ⁵R. G. Giovanelli, *Nature* **158**, 81 (1946).
- ⁶S. Tsuneta, *Astrophys. J.* **456**, 840 (1996).
- ⁷D. N. Baker, T. I. Pulkkinen, V. Angelopoulos, W. Baumjohann, and R. L. McPherron, *J. Geophys. Res.* **101**, 12975, doi:10.1029/95JA03753 (1996).
- ⁸T. Nagai, M. Fujimoto, Y. Saito, S. Machida, T. Terasawa, R. Nakamura, T. Yamamoto, T. Mukai, A. Nishida, and S. Kokubun, *J. Geophys. Res.* **103**, 4419, doi:10.1029/97JA02190 (1998).
- ⁹V. Angelopoulos, J. P. McFadden, D. Larson, C. W. Carlson, S. B. Mende, H. Frey, T. Phan, D. G. Sibeck, K.-H. Glassmeier, U. Auster, E. Donovan, I. R. Mann, I. J. Rae, C. T. Russell, A. Runov, X.-Z. Zhou, and L. Kepko, *Science* **321**, 931 (2008).
- ¹⁰J. A. Wesson, *Nucl. Fusion* **30**, 2545 (1990).

- ¹¹M. Yamada, F. M. Levinton, N. Pomphrey, R. Budny, J. Manickam, and Y. Nagayama, *Phys. Plasmas* **1**, 3269 (1994).
- ¹²M. Hoshino, T. Mukai, T. Terasawa, and I. Shinohara, *J. Geophys. Res.* **106**, 25979, doi:10.1029/2001JA900052 (2001).
- ¹³J. F. Drake, M. A. Shay, W. Thongthai, and M. Swisdak, *Phys. Rev. Lett.* **94**, 095001 (2005).
- ¹⁴X. R. Fu, Q. M. Lu, and S. Wang, *Phys. Plasmas* **13**, 012309 (2006).
- ¹⁵P. L. Pritchett, *Geophys. Res. Lett.* **33**, L13104, doi:10.1029/2005GL025267 (2006).
- ¹⁶K. Fujimoto and R. D. Sydora, *Phys. Plasmas* **16**, 112309 (2009).
- ¹⁷C. Huang, Q. M. Lu, and S. Wang, *Phys. Plasmas* **17**, 072306 (2010).
- ¹⁸J. Egedal, W. Daughton, and A. Le, *Nat. Phys.* **8**, 321 (2012).
- ¹⁹H. Y. Wang, Q. M. Lu, C. Huang, and S. Wang, *Astrophys. J.* **821**, 84 (2016).
- ²⁰M. Øieroset, R. P. Lin, T. D. Phan, D. E. Larson, and S. D. Bale, *Phys. Rev. Lett.* **89**, 195001 (2002).
- ²¹S. Imada, R. Nakamura, P. W. Daly, M. Hoshino, W. Baumjohann, S. Mühlbacher, A. Balogh, and H. Reme, *J. Geophys. Res.* **112**, A03202, doi:10.1029/2006JA011847 (2007).
- ²²L. J. Chen, A. Bhattacharjee, P. A. Puhl-Quinn, H. Yang, N. Bessho, S. Imada, S. Mühlbacher, P. W. Daly, B. Lefebvre, Y. Khotyaintsev, A. Vaivads, A. Fazakerley, and E. Georgescu, *Nat. Phys.* **4**, 19 (2008).
- ²³R. S. Wang, Q. M. Lu, C. Huang, and S. Wang, *J. Geophys. Res.* **115**, A01209, doi:10.1029/2009JA014553 (2010).
- ²⁴R. S. Wang, Q. M. Lu, A. M. Du, and S. Wang, *Phys. Rev. Lett.* **104**, 175003 (2010).
- ²⁵R. S. Wang, Q. M. Lu, X. Li, C. Huang, and S. Wang, *J. Geophys. Res.* **115**, A11201, doi:10.1029/2010JA015473 (2010).
- ²⁶S. Y. Huang, A. Vaivads, Y. V. Khotyaintsev, M. Zhou, H. S. Fu, A. Retino, X. H. Deng, M. Andre, C. M. Cully, J. S. He, F. Sahraoui, Z. G. Yuan, and Y. Pang, *Geophys. Res. Lett.* **39**, L11103, doi:10.1029/2012GL051946 (2012).
- ²⁷H. S. Fu, Y. V. Khotyaintsev, A. Vaivads, A. Retino, and M. Andre, *Nat. Phys.* **9**, 426 (2013).
- ²⁸W. Daughton, J. Scudder, and H. Karimabadi, *Phys. Plasmas* **13**, 072101 (2006).
- ²⁹H. Karimabadi, W. Daughton, and J. Scudder, *Geophys. Res. Lett.* **34**, L13104, doi:10.1029/2007GL030306 (2007).
- ³⁰M. A. Shay, J. F. Drake, and M. Swisdak, *Phys. Rev. Lett.* **99**, 155002 (2007).
- ³¹T. D. Phan, J. F. Drake, M. A. Shay, F. S. Mozer, and J. P. Eastwood, *Phys. Rev. Lett.* **99**, 255002 (2007).
- ³²J. F. Drake, M. A. Shay, and M. Swisdak, *Phys. Plasmas* **15**, 042306 (2008).
- ³³Q. M. Lu, C. Huang, J. L. Xie, R. S. Wang, M. Y. Wu, A. Vaivads, and S. Wang, *J. Geophys. Res.* **115**, A11208, doi:10.1029/2010JA015713 (2010).
- ³⁴P. M. Nilson, L. Willingale, M. C. Kaluza, C. Kamperidis, S. Minardi, M. S. Wei, P. Fernandes, M. Notley, S. Bandyopadhyay, M. Sherlock, R. J. Kingham, M. Tatarakis, Z. Najmudin, W. Rozmus, R. G. Evans, M. G. Haines, A. E. Dangor, and K. Krushelnick, *Phys. Rev. Lett.* **97**, 255001 (2006).
- ³⁵P. M. Nilson, L. Willingale, M. C. Kaluza, C. Kamperidis, S. Minardi, M. S. Wei, P. Fernandes, M. Notley, S. Bandyopadhyay, M. Sherlock, R. J. Kingham, M. Tatarakis, Z. Najmudin, W. Rozmus, R. G. Evans, M. G. Haines, A. E. Dangor, and K. Krushelnick, *Phys. Plasmas* **15**, 092701 (2008).
- ³⁶L. Willingale, P. M. Nilson, M. C. Kaluza, A. E. Dangor, R. G. Evans, P. Fernandes, M. G. Haines, C. Kamperidis, R. J. Kingham, C. P. Ridgers, M. Sherlock, A. G. R. Thomas, M. S. Wei, Z. Najmudin, K. Krushelnick, S. Bandyopadhyay, M. Notley, S. Minardi, M. Tatarakis, and W. Rozmus, *Phys. Plasmas* **17**, 043104 (2010).
- ³⁷C. K. Li, F. H. Séguin, J. A. Frenje, J. R. Rygg, R. D. Petrasso, R. P. J. Town, P. A. Amendt, S. P. Hatchett, O. L. Landen, A. J. Mackinnon, P. K. Patel, M. Tabak, J. P. Knauer, T. C. Sangster, and V. A. Smalyuk, *Phys. Rev. Lett.* **99**, 015001 (2007).
- ³⁸M. J. Rosenberg, C. K. Li, W. Fox, I. Igumenshchev, F. H. Séguin, R. P. J. Town, J. A. Frenje, C. Stoeckl, V. Glebov, and R. D. Petrasso, *Nat. Commun.* **6**, 6190 (2015).
- ³⁹J. Zhong, Y. T. Li, X. G. Wang, J. Q. Wang, Q. L. Dong, C. J. Xiao, S. J. Wang, X. Liu, L. Zhang, L. An, F. L. Wang, J. Q. Zhu, Y. Gu, X. T. He, G. Zhao, and J. Zhang, *Nat. Phys.* **6**, 984 (2010).
- ⁴⁰Q. L. Dong, S. J. Wang, Q. M. Lu, C. Huang, D. W. Yuan, X. Liu, X. X. Lin, Y. Li, H. G. Wei, J. Zhong, J. R. Shi, S. E. Jiang, Y. K. Ding, B. B. Jiang, K. Du, X. T. He, M. Y. Yu, C. S. Liu, S. Wang, Y. J. Tang, J. Q. Zhu, G. Zhao, Z.-M. Sheng, and J. Zhang, *Phys. Rev. Lett.* **108**, 215001 (2012).

- ⁴¹W. Fox, A. Bhattacharjee, and K. Germaschewski, *Phys. Rev. Lett.* **106**, 215003 (2011).
- ⁴²S. Lu, Q. M. Lu, Q. L. Dong, C. Huang, S. Wang, J. Q. Zhu, Z.-M. Sheng, and J. Zhang, *Phys. Plasmas* **20**, 112110 (2013).
- ⁴³Q.-L. Dong, D.-W. Yuan, S.-J. Wang, Y. T. Li, X. Liu, S. E. Jiang, Y. K. Ding, K. Du, M.-Y. Yu, X.-T. He, Y. J. Tang, J. Q. Zhu, G. Zhao, Z.-M. Sheng, and J. Zhang, *J. Plasma Phys.* **78**, 497 (2012).
- ⁴⁴S. Lu, Q. M. Lu, C. Huang, Q. L. Dong, J. Q. Zh, Z.-M. Sheng, S. Wang, and J. Zhang, *New J. Phys.* **16**, 083021 (2014).
- ⁴⁵W. Fox, A. Bhattacharjee, and K. Germaschewski, *Phys. Plasmas* **19**, 056309 (2012).
- ⁴⁶S. Lu, Q. M. Lu, F. Guo, Z. M. Sheng, H. Y. Wang, and S. Wang, *New J. Phys.* **18**, 013051 (2016).
- ⁴⁷Z. Xu, B. Qiao, H. X. Chang, W. P. Yao, S. Z. Wu, X. Q. Yan, C. T. Zhou, X. G. Wang, and X. T. He, *Phys. Rev. E* **93**, 033206 (2016).
- ⁴⁸H. Karimabadi, J. Dorelli, H. X. Vu, B. Loring, and Y. Omelchenko, *AIP Conf. Proc.* **1320**, 137–143 (2011).
- ⁴⁹J. Scudder and W. Daughton, *J. Geophys. Res.* **113**, A06222, doi:10.1029/2008JA013035 (2008).
- ⁵⁰J. Egedal, W. Daughton, A. Li, and A. L. Borg, *Phys. Plasmas* **22**, 101208 (2015).
- ⁵¹C. Huang, M. Wu, Q. Lu, R. Wang, and S. Wang, *J. Geophys. Res.* **120**, 1759, doi:10.1002/2014JA020918 (2015).
- ⁵²M. J. Rosenberg, C. K. Li, W. Fox, A. B. Zylstra, C. Stoeckl, F. H. Séguin, J. A. Frenje, and R. D. Petrasso, *Phys. Rev. Lett.* **114**, 205004 (2015).